TITLE

PELP1/SRC-3-dependent regulation of metabolic kinases drives therapy resistant ER+ breast cancer

AUTHORS

Thu H. Truong[1], Elizabeth A. Benner[1], Kyla M. Hagen[1], Nuri A. Temiz[1,4], Carlos Perez Kerkvliet[1], Ying Wang[1], Thomas Pengo[5], Katrin P. Guillen[6,8], Bryan W. Welm[6,7,8], Sucheta Telang[9], *Carol A. Lange[1,2,3], and *Julie H. Ostrander[1,2]

* co-senior authors

AFFILIATIONS

[1] Masonic Cancer Center, [2] Department of Medicine (Division of Hematology, Oncology, and Transplantation), [3] Department of Pharmacology, [4] Institute for Health Informatics, and [5] University of Minnesota Informatics Institute, University of Minnesota, Minneapolis MN 55455 USA

[6] Department of Oncological Sciences, [7] Department of Surgery, and [8] Huntsman Cancer Institute, University of Utah, Salt Lake City UT 84112,

[9] James Graham Brown Cancer Center, Department of Medicine (Division of Medical Oncology and Hematology), University of Louisville, Louisville KY 40202 USA

ABSTRACT

Recurrence of metastatic breast cancer stemming from acquired endocrine and chemotherapy resistance remains a health burden for women with luminal (ER+) breast cancer. Disseminated ER+ tumor cells can remain viable but quiescent for years to decades. Contributing factors to metastatic spread include the maintenance and expansion of breast cancer stem cells (CSCs). Breast CSCs frequently exist as a minority population in therapy resistant tumors. In this study, we show that cytoplasmic complexes composed of steroid receptor (SR) co-activators, PELP1 and SRC-3, modulate breast CSC expansion through upregulation of the HIF-activated metabolic target genes *PFKFB3* and *PFKFB4*. Seahorse metabolic assays demonstrated that cytoplasmic PELP1 influences cellular metabolism by increasing both glycolysis and mitochondrial respiration. PELP1 interacts with PFKFB3 and PFKFB4 proteins, and inhibition of PFKFB3 and PFKFB4 kinase activity blocks PELP1-induced tumorspheres and protein-protein interactions with SRC-3. PFKFB inhibitors exhibited combinatorial effects in conjunction with ER targeted therapies in breast cancer cells, including tamoxifen resistant (TamR) and paclitaxel resistant (TaxR) models and ER+ patient-derived organoids (PDxO). Finally, PFKFB4 knockdown resulted in decreased circulating tumor cell (CTC) populations in mammary intraductal (MIND) models. Together, our data suggest that PELP1, SRC-3, and PFKFBs cooperate to drive ER+ tumor cell populations that include CSCs and CTCs. Identifying non-ER pharmacological targets offers a useful approach to blocking metastatic escape from standard of care ER/estrogen (E2)-targeted strategies to overcome endocrine and chemotherapy resistance.

INTRODUCTION

Metastatic recurrence is an incurable but common complication of ER+ breast cancer. Treatment of metastatic breast cancer typically results in endocrine resistance and chemotherapy is largely ineffective. Altered signaling pathways drive therapy resistance and offer potential targets for metastatic ER+ breast cancer. Studies have shown that endocrine resistance is independently driven by PELP1 (proline, glutamic acid, leucine-rich protein 1) and SRC-3 (steroid receptor [SR] co-activator-3). PELP1 and SRC-3 are both SR co-activators involved in normal development and cancer (1,2). Increased PELP1 expression is associated with higher tumor grade, tumor proliferation, and decreased breast cancer-specific survival (3,4). PELP1 is primarily nuclear in normal breast tissue; however, altered cytoplasmic PELP1 localization is observed in 40-58% of PELP1+ breast tumors (5). Analysis of breast tumor samples revealed that patients with high cytoplasmic PELP1 levels were less likely to respond to tamoxifen (tam) (4). Similarly, SRC-3

mRNA and protein overexpression are correlated with higher tumor grade and decreased overall and disease-free survival (6). SRC-3 overexpression is also linked to tam resistance in breast cancer models and human breast tumors (7,8). Both PELP1 and SRC-3 have essential nuclear functions, but also dynamically shuttle to the cytoplasm where they associate with signaling molecules and act as scaffolds for growth factor or SR pathways. These SR co-activators have emerged as promising targets in ER+ breast cancer and as potential mediators of therapy resistance.

Cancer stem cells (CSCs) are poorly proliferative and frequently exist as a minority sub-population of cells that drive therapy resistance and metastasis (9). In contrast to non-CSCs, breast CSCs form colonies in serum-free suspension culture (i.e. tumorspheres), express stem cell markers (e.g. ALDH+ or $CD44^{hi}/CD24^{lo}$), exhibit enhanced resistance to chemo and endocrine therapies, and express markers of epithelial to mesenchymal transition (EMT). The ability to survive and self-renew following treatment allows CSCs to evade standard chemo and endocrine therapies aimed at rapidly dividing cancer cells and to drive metastatic tumor growth.

Growing evidence has implicated SR co-activators as mediators of CSC self-renewal. For example, SRC-3 drives CSC formation and tumor outgrowth in breast cancer models. Treatment with SI-2, an SRC-3 inhibitor, decreased SRC-3-induced CSC formation in breast cancer cell and xenograft models (10). Our laboratory reported that cytoplasmic complexes composed of PELP1 and SRC-3 mediate breast CSC expansion (11). Targeting SRC-3 using shRNA or pharmacological inhibitors (i.e. SI-2) abrogated PELP1/SRC-3 complex formation, PELP1-induced tumorspheres, and expression of PELP1 target genes that promote cancer cell survival. These studies imply that inhibiting PELP1 and its binding partners may provide a way to target the breast CSC population in order to improve patient outcomes.

Herein we sought to identify mechanisms that contribute to PELP1-driven CSC survival and self-renewal in ER+ breast cancer. Using endocrine and chemotherapy resistant breast cancer models, our findings suggest that PELP1/SRC-3 complexes modulate the CSC compartment through gene programs associated with metabolic adaptation. Importantly, we demonstrate rational combinations of inhibitors that target PELP1-binding partners and/or endocrine therapies reduced CSC populations in preclinical patient-derived organoid (PDxO) models. Furthermore, knockdown of PELP1 binding partners reduced circulating tumor cells (CTC) in mouse mammary intraductal (MIND) xenografts *in vivo*. In contrast to current therapies that fail to adequately target

slow-growing breast CSCs, our studies reveal therapy combinations that inhibit cooperating signaling cascades, while simultaneously targeting ER. By targeting CSCs directly, this approach promises to significantly improve the lives of patients with recurrent ER+ breast cancer.

MATERIALS AND METHODS

Cell Culture. STR authentication was performed by ATCC (October 2018). MCF-7 PELP1 and J110 cells were cultured as described (11). MCF-7 (12) and T47D TamR (13) cells were cultured in 100 nM tamoxifen. MCF-7 TaxR (14) cells were cultured in 2 μM Taxol. For 3D (tumorsphere) conditions, cells were cultured as described (11).

Seahorse Assays. Seahorse XFe96 Analyzer (Agilent) was used to measure ECAR and OCR levels. MCF-7 PELP1 cells were seeded into Agilent XF96 culture plates (2.5×10^4 cells/well with 22.4 μg/ml Cell Tak) and incubated at 37 °C for 24 h. Cells were washed 2x and incubated in Seahorse XF DMEM media (2 mM L-glutamine, 11.11 mM glucose, 1.0 mM sodium pyruvate; pH 7.4) at 37 °C in a CO_2-free incubator for 45 min. ECAR and OCR were detected under basal conditions followed by addition of 0.5 μM FCCP and 2 μM oligomycin using the XF Cell Energy Phenotype and Mito Stress Test (Agilent). Protein concentrations were measured by BCA Assay following addition of RIPA-lite (25 μl/well). ECAR and OCR data were normalized to total protein concentration per well. Data are presented as the average ± SD of experimental triplicates. MCF-7 TaxR cell conditions: 1×10^4 cells/well, Seahorse XF DMEM media (2 mM L-glutamine, 5.55 mM glucose, 1 mM sodium pyruvate; pH 7.4), FCCP (0.25-0.5 μM), and oligomycin (2 μM).

Glucose Uptake. Glucose uptake was measured using 2-NBDG (Thermo Fisher). Cells were incubated in glucose-free DMEM containing 1% HEPES (Gibco) for 15 min and then treated with 2-NBDG for 25 min at 37 °C. Cells were dissociated using trypsin, washed, and resuspended in cold FACS buffer (D-PBS containing 2% FBS). 2-NBDG fluorescence was quantified by flow cytometry, and sorting gates were established using untreated control cells.

Patient-Derived Organoids (PDxO). PDxOs (HCI-003, HCI-017) were cultured in Advanced DMEM/F12 (Thermo Fisher) containing 5% FBS, 1X HEPES, 1X GlutaMax, 50 μg/ml Gentamicin (Genesee), 1 μg/ml hydrocortisone, 10 ng/ml EGF, and supplemented with 10 μM Y-27632 (Selleckchem), 100 ng/ml FGF2 (PeproTech), and 1 mM N-acetyl cysteine (Sigma). PDxOs were embedded into Matrigel (growth factor reduced; Corning) and passaged every ~14-18 days.

Mammary Intraductal (MIND) Model. Intraductal injections of single cells were performed as described (15,16). Seven-week old female NSG mice were purchased from Jackson Laboratory. Five mice/group were injected with 5 x 10^4 cells into each nipple of the 4th inguinal glands with the indicated breast cancer cell line. Mammary glands were harvested 8 weeks after injection, fixed in 4% PFA, and processed for H&E staining. H&E sections were analyzed using ImageJ or Q-path to quantitate the total mammary gland area (%) that contained tumor cells.

CTC Soft Agar Assays. Fresh mouse blood samples were processed using Isolymph/Ficoll-Paque (Sigma). Buffy coat containing circulating tumor cells was seeded into DMEM containing 5% FBS, 1X sterile low melt agarose (Thermo Fisher), and 1X penicillin streptomycin. Colonies were grown for 14 days at 37 °C. Data are presented as the average ± SD of five independent measurements.

Statistical Analysis. Data were tested for normal distribution using Shapiro-Wilks normality test and homogeneity of variances using Bartlett's Test. Once data met these two requirements, statistical analyses were performed using one-way or two-way ANOVA in conjunction with Tukey multiple comparison test for means between more than two groups or Student *t* test for means between two groups, where significance was determined with 95% confidence. For the MIND study with four groups defined by two factors (cyto PELP1 vs. WT PELP1, and shPFKFB4 vs. shGFP), a regression model identified a significant interaction due to shPFKFB4 at an alpha level of 0.1 (p=0.084).

RESULTS

Cytoplasmic PELP1 promotes CSCs and HIF-regulated gene expression

Breast CSCs represent a minority of the total cell population (1-5%) (17), making it difficult to detect CSC-specific changes in heterogeneous populations. We therefore measured breast CSC frequency by comparing ALDH activity (**Figure 1A**, **Supplementary Figure 1**) and CD44^{hi}/CD24^{lo} ratios (**Figure 1B**, **Supplementary Figure 2**) in MCF-7 cells stably expressing LXSN (vector control), WT PELP1, or cytoplasmic (cyto) PELP1 cultured in either 2D (adherent) or 3D (tumorsphere) conditions. Relative to 2D, 3D conditions increased breast CSC markers in MCF-7 cells expressing LXSN, WT PELP1, or cyto PELP1 (**Figure 1A, 1B**). In 2D conditions, cyto PELP1 expressing cells had no significant changes in ALDH activity when compared to LXSN or

WT PELP1; however, 3D conditions significantly increased ALDH activity in cells expressing cyto PELP1 (12.0% ± 2.9) compared to LXSN (6.6% ± 0.67, p = 0.023) and WT PELP1 (2.6% ± 0.76, p = 0.0015). In 2D conditions, $CD44^{hi}/CD24^{lo}$ populations were increased in cyto PELP1 expressing cells (13.0% ± 0.49) compared to LXSN (2.6% ± 0.042, p < 0.0001) or WT PELP1 (1.2% ± 0.19, p < 0.0001), and this trend was enhanced in 3D conditions (cyto PELP1, 19.4% ± 1.4; LXSN, 9.0% ± 1.1, p = 0.0045; WT PELP1, 2.3% ± 0.18, p = 0.0011). WT PELP1 displayed lower ALDH activity and $CD44^{hi}/CD24^{lo}$ ratios relative to LXSN controls, suggesting that nuclear PELP1 limits CSC behavior. These results indicate that both 3D culture and cyto PELP1 expression independently increase CSC expansion in MCF-7 cell models.

We performed RNA-seq on MCF-7 PELP1 models grown as 3D tumorspheres and compared these data to studies conducted in 2D culture (11) to identify candidate genes and pathways differentially regulated in cyto PELP1 expressing cells. Comparison of 3D versus 2D conditions identified 206 upregulated and 114 downregulated genes similarly regulated by >2-fold in all cell lines (LXSN, WT PELP1, cyto PELP1) (**Figure 1C, Supplementary Figure 3**). Ingenuity Pathway Analysis (IPA) of these 320 genes revealed activation of estrogen, growth factor, cytokine, and NF-κB pathways (**Supplementary Table 1**). Significantly activated and inhibited "Diseases and Functions" are summarized in **Supplementary Table 2**. 3D to 2D comparison in cyto PELP1 expressing cells identified 173 differentially expressed genes (93 upregulated, 80 downregulated) compared to LXSN or WT PELP1 (**Figure 1C, Supplementary Figure 4**). These 173 genes were analyzed with IPA to identify cyto PELP1-specific pathways (**Figure 1D**), biological functions, or disease states (**Figure 1E**), and predicted increased HIF activation, estradiol, ATF4, and glycolytic-mediated pathways. We created representative heatmaps to illustrate 3D-specific regulation in upstream regulator analysis associated with HIF and ATF4 pathway activation (>2-fold; **Figure 1F**) and generated a cyto PELP1 upregulated gene signature (**Supplementary Table 3**). Volcano plots of differentially regulated genes are shown in **Figure 1G**; red dots indicate genes in the cyto PELP1 signature. We then used the cyto PELP1 upregulated gene signature to query the METABRIC breast cancer database. Higher expression of this gene signature was associated with lower overall survival (OS) in the METABRIC cohort (hazard ratio = 1.485, p < 0.0001, **Figure 1H**). We tested this on the ER+ only subtype within the METABRIC cohort and found similar results (hazard ratio = 1.483, p < 0.0001, **Figure 1I**). A similar query of the TCGA database revealed no significant differences in OS (**Supplementary Figure 5**). Taken together, these data identify genes involved in cyto PELP1-mediated pathways that promote CSCs, including those associated with HIF-activated and glycolytic pathways.

205

206 **Cytoplasmic PELP1 drives metabolic plasticity**

207 Next, we validated cyto PELP1 induced genes identified in our RNA-seq analysis. HIF activates
208 the *PFKFB* family, which are metabolic bi-functional kinase/phosphatases (18). We found that
209 mRNA levels of *EPAS1* (i.e. HIF2α), *PFKFB3*, and *PFKFB4* were upregulated in cells expressing
210 cyto PELP1 relative to LXSN or WT PELP1 in 3D, but not 2D conditions (**Figure 2A**). Additional
211 validation of HIF-activated metabolic and stem cell genes include *NDRG1* and *SOX9* (**Figure 2A**).
212 Given the central role of HIF pathways in metabolism (19), we investigated the effect of PELP1
213 on metabolic pathways using the Seahorse Cell Energy Phenotype test to measure oxygen
214 consumption rate (OCR) and extracellular acidification rate (ECAR). At baseline, MCF-7 cells
215 expressing cyto PELP1 exhibited a significant increase in OCR levels compared to LXSN and WT
216 PELP1. Under stressed conditions (i.e. after FCCP and oligomycin), OCR was increased in cyto
217 PELP1 expressing cells compared to LXSN ($p = 0.0096$). ECAR was significantly different in cyto
218 PELP1 expressing cells compared to LXSN at baseline, but WT and cyto PELP1 displayed an
219 increase in ECAR compared to LXSN controls ($p = 0.046$ and 0.0045) under stressed conditions
220 (**Figure 2B**). To systematically test effects on key parameters of mitochondrial function, we
221 performed the Seahorse Mito Stress test. Cyto PELP1 expression significantly increased basal
222 respiration, compared to LXSN and WT PELP1 ($p < 0.0001$ and 0.0001). Furthermore, cyto
223 PELP1 increased ATP-linked respiration, proton leak, maximal respiration, and non-mitochondrial
224 respiration (**Figure 2C**). Cyto PELP1 expressing cells had a 4-fold increase in glucose uptake
225 compared to WT PELP1 and LXSN, as measured by 2-NBDG (**Figure 2D, Supplementary**
226 **Figure 7**). Collectively, these results indicate cyto PELP1 drives gene expression associated with
227 HIF-activated metabolic programs (i.e. *PFKFB3*, *PFKFB4*) in 3D culture, and affects mitochondrial
228 respiration and glycolysis, indicative of metabolic plasticity.

229

230 **Inhibition of PFKFBs disrupts PELP1/SRC-3 complexes and tumorsphere formation**

231 We hypothesized PFKFB3 and PFKFB4 are required components of the PELP1/SRC-3 complex.
232 Co-immunoprecipitation of PFKFB3 or PFKFB4 demonstrated increased association with PELP1
233 in cells expressing cyto PELP1 relative to LXSN or WT PELP1 (**Figure 3A, 3B**). Treatment with
234 PFK158 and 5MPN, inhibitors of PFKFB3 and PFKFB4 respectively, reduced the PELP1/SRC-3
235 interaction (**Figure 3C, 3D**). These inhibitors also blocked PELP1/PFKFB3 and PELP1/PFKFB4
236 (**Supplementary Figure 8A, 8B**) interactions in cyto PELP1 expressing cells; similar results were
237 observed with another PFKFB3 inhibitor (PFK15; **Supplementary Figure 8C, 8D**).

238

Next, we tested the effect of PFKFB inhibition on cyto PELP1-induced tumorspheres. PFKFB4 knockdown (**Supplementary Figure 9**) decreased tumorsphere formation in cyto PELP1 expressing cells by ~50%, but not in LXSN or WT PELP1 (**Figure 3E**, p = 0.0103). Attempts to stably knockdown PFKFB3 were not successful, suggesting that PFKFB3 is crucial for cell viability (20). Inhibitors of PFKFB3 and PFKFB4 reduced cyto PELP1-induced tumorspheres, but had no effect on cells expressing either LXSN or WT PELP1. (**Figure 3F, 3G; Supplementary Figure 8E**). To evaluate PFKFB inhibitors in an alternative PELP1/SRC-3 model, we used a murine tumor cell line (J110) established from the MMTV-SRC-3 mouse (21). Similar to MCF-7 PELP1 models, PFK158 or 5MPN inhibited tumorsphere formation by ~40% in J110 cells (**Figure 3H**). Western blotting indicated that PFKFB3 and PFKFB4 protein levels remained unchanged in response to E2, while ER levels decreased, presumably due to ligand-induced turnover (**Figure 3H,** right). These results indicate that blocking PFKFB3 or PFKFB4 through knockdown or pharmacological inhibition disrupts expansion and self-renewal of PELP1-driven CSC populations.

Targeting PELP1/SRC-3 complexes in therapy resistant cell lines

Paclitaxel (Taxol) is a chemotherapy used to treat late stage breast cancer. Increased PELP1, HIF1α, and HIF-2α expression has been observed in triple negative breast cancer (TNBC) cells in response to Taxol (14). To evaluate whether PELP1 expression affects response to Taxol in ER+ breast cancer, we treated MCF-7 PELP1 cells (LXSN, WT PELP1, cyto PELP1) cultured as tumorspheres with Taxol (0 to 125 nM). We assessed tumorsphere formation and calculated IC50 values for each cell line (**Figure 4A**). IC50 (Taxol) for cyto PELP1 expressing cells was ~2-fold higher than LXSN or WT PELP1. These results suggest that cyto PELP1 expression confers enhanced Taxol resistance compared to LXSN or WT PELP1.

Next, we determined if PELP1/SRC-3 signaling mediates therapy resistance in tamoxifen resistant (TamR) and paclitaxel-resistant (TaxR) cell lines. *EPAS1, PFKFB3, and PFKFB4* mRNA levels were increased in MCF-7 TaxR (**Figure 4B,** *top*) and TamR cells (**Figure 4B,** *bottom*) relative to MCF-7 parental controls, particularly in 3D conditions. 3D PELP1 target genes, *NDRG1* and *SOX9* were also upregulated in TaxR and TamR cells relative to parental MCF-7 cells (**Supplementary Figure 6**). To determine if similar changes in cellular metabolism occur in MCF-7 TaxR models, we performed Seahorse metabolic assays. The Cell Energy Phenotype test showed TaxR cells exhibit increased OCR and ECAR at baseline and stressed conditions relative to controls (**Figure 4C**), indicating increased mitochondrial respiration and glycolysis. To look at individual effects on OCR, we performed the Mito Stress test in MCF-7 TaxR models. Similar to

cyto PELP1 expressing cells, TaxR cells showed significant increases in basal and maximal respiration compared to controls (**Figure 4D**). TaxR cells increased proton leak, spare respiratory capacity, and non-mitochondrial respiration, but not ATP production as observed in MCF-7 cyto PELP1 expressing cells. TaxR cells also displayed ~2-fold increase ($p = 0.0006$) in glucose uptake compared to controls (**Figure 4E**). Together, these data reveal that TamR and TaxR models phenocopy HIF-associated target gene expression and metabolic plasticity of MCF-7 cyto PELP1 expressing cells, and suggest PELP1 may be a key mediator in therapy resistance.

We found that the PELP1/SRC-3 interaction was similarly increased in MCF-7 TaxR (**Figure 4F**, top) and TamR cells (**Figure 4F**, bottom). Additionally, $CD44^{hi}/CD24^{lo}$ ratios were increased in MCF-7 TaxR cells compared to parental controls (**Supplementary Figure 10**). To test the pharmacological effect of PFKFB3, PFKFB4, and SRC-3 inhibition, MCF-7 TaxR and TamR cells were seeded as tumorspheres and treated with PFK158, 5MPN, and SI-2. Both resistant models exhibited increased basal tumorsphere formation when compared to parental controls. 5MPN and SI-2 effectively decreased secondary tumorsphere formation by 71% and 75% in TaxR (**Figure 4G**), and 88% and 92% in TamR models (**Figure 4H**) compared to vehicle controls. PFK158 (PFKFB3 inhibitor) modestly decreased TaxR and TamR tumorspheres by 17% and 27%. These findings highlight the overlap of key players involved in PELP1-driven CSC biology and suggest that PFKFB4 and SRC-3 play a more significant role than PFKFB3 within resistant cell models.

We hypothesized that tam in combination with PELP1/SRC-3 complex inhibitors (i.e. SI-2 or 5MPN) would be more effective than either inhibitor alone. Combination treatments were evaluated in several cell lines. In MCF-7 PELP1 models, we tested tam/SI-2, tam/5MPN, and SI-2/5MPN combinations (**Figure 5A-5C**). Tam/SI-2 and tam/5MPN reduced tumorsphere formation in cyto PELP1 expressing cells by ~85% ($p < 0.0001$) and 80% ($p < 0.0001$) compared to vehicle. Single agent treatment with tam or SI-2 also reduced tumorsphere, but to a lesser degree than combinations. PFK158 co-treatment with tam was not more effective than tam alone and was not further pursued (**Supplementary Figure 11A**). Effective combinations were then tested in J110 cells (**Supplementary Figure 11B-11D**). Tam, SI-2, and 5MPN alone inhibited tumorspheres by 39, 41, and 28%, while co-treatment did not have dramatic effects. The SI-2/5MPN combination was most effective in J110 cells, and decreased tumorsphere formation by 60%, most likely because J110 cells are an SRC-3-derived transgenic mouse mammary tumor cell line (22).

Because PELP1 confers tamoxifen and Taxol resistance (**Figure 4A**), we also tested the effect of these agents in resistant cell models. Similar to observations in MCF-7 PELP1 models, tam co-treatments were more effective when combined with SI-2 or 5MPN in MCF-7 TaxR models (**Figure 5D, 5E**). The SI-2/5MPN combination was not more effective than individual agents in TaxR models (**Figure 5F**), suggesting that SRC-3 and PFKFB4 cooperation occurs in tam-sensitive models. Accordingly, SI-2/5MPN co-treatment in MCF-7 and T47D TamR models reduced tumorsphere formation by 77% ($p < 0.0001$) and 75% ($p < 0.0001$) (**Supplementary Figure 11E, 11F**). These studies provide promising alternative approaches to target non-ER mediators and overcome emergence of chemotherapy and endocrine resistance.

Targeting PELP1/SRC-3 complexes in PDxO and MIND models

To explore the therapeutic potential of inhibitor combinations, we utilized pre-clinical patient-derived organoid models (PDxO; (23)). First, we identified two ER+ PDxO models (HCI-003, HCI-017) that express PELP1, SRC-3, PFKFB3, PFKFB4, and ER based on mRNA and protein levels (**Supplementary Figure 12, Figure 6A**). MCF-7 and T47D cell lines were included as controls. We tested effective combinations identified from **Figure 5** on CSC expansion in PDxO models. PDxOs were grown to maturity, pre-treated for 3 days, then dissociated and seeded into tumorspheres in the presence of inhibitors. Individual treatments (tam, SI-2, 5MPN) reduced tumorsphere formation in both PDxO models by 36 to 62% (**Figure 6B-6D**). The tam/SI-2 combination was not more effective than individual treatment (**Figure 6B**). In contrast, tam/5MPN was more effective than tam or 5MPN alone and reduced tumorspheres by ~71% and ~90% in HCI-003 and HCI-017 (**Figure 6C**)**.** SI-2/5MPN co-treatment was more effective than SI-2 or 5MPN alone and reduced tumorsphere formation by ~71% ($p < 0.0001$) and ~74% ($p < 0.0001$) in HCI-003 and HCI-017 (**Figure 6D**). These results demonstrate that blocking the PELP1/SRC-3 complex and associated binding partners is an effective approach to targeting CSC populations in pre-clinical PDxO models.

To evaluate if PELP1 promotes tumor formation, we injected MCF-7 WT and cyto PELP1 expressing cells (5×10^4) into the inguinal mammary glands of adult female mice (6-8 week old, 4 mice/group) to generate mammary intraductal (MIND) tumors. Both cell lines had 100% engraftment rates (**Figure 7A, Supplementary Figure 13**). Tumor area (%) was calculated from H&E images of each mammary gland and was increased in cyto PELP1 ($25.7\% \pm 16.5$) compared to WT PELP1 tumors ($10.9\% \pm 9.5$, $p = 0.046$) (**Figure 7B**).

Our PDxO data showed that 5MPN co-treatment with SI-2 or tam decreased tumorspheres. We queried PFKFB4 mRNA levels on OS in METABRIC datasets. High PFKFB4 mRNA expression is associated with decreased OS in all subtypes and ER+ only patient cohorts (**Supplementary Figure 14**). Therefore, we tested whether PFKFB4 knockdown would impact MIND tumor growth or the presence of circulating tumor cells (CTCs); a marker of metastatic potential and associated CSC behavior (24,25). 5 mice/group were injected with MCF-7 WT and cyto PELP1 expressing cells (shGFP control or shPFKFB4). 8 weeks post-injection, mammary glands were fixed and processed for H&E staining (**Supplementary Figure 15**). As in **Figure 7B**, the difference in means between WT PELP1 shGFP (26.8% ± 10.2) and cyto PELP1 shGFP (41.2% ± 17.2) tumor area was significant ($p = 0.036$, **Figure 7C**). Knockdown of PFKFB4 in MCF-7 cells expressing WT PELP1 or cyto PELP1 did not have a significant effect on primary tumor growth. To assess disseminated tumor cells, blood samples were collected during euthanization and seeded into soft agar assays to detect CTCs. Mice injected with WT PELP1 (shGFP or shPFKFB4) expressing cells did not exhibit CTC colony formation. In sharp contrast, blood samples from mice engrafted with cyto PELP1 cells developed colonies, indicating the presence of CTCs. Knockdown of shPFKFB4 in MCF-7 cyto PELP1 expressing cells reduced colony formation ($p < 0.0492$) and colony size ($p < 0.0016$) (**Figure 7D-7F**). These data demonstrate a requirement for PFKFB4 in cyto PELP1-driven CTC formation and expansion *in vivo*.

DISCUSSION

The CSC hypothesis postulates that tumors contain a subset population (i.e. CSCs) that share properties of normal stem cells including self-renewal, differentiation, and capacity to repopulate the heterogeneous tumor (9). CSCs are proposed to have heightened resistance to cancer therapies due to their relative quiescent state (26), enabling this population to evade standard of care treatments that target proliferating bulk tumor cells. Herein, we sought to define mechanisms of SR co-activator driven CSC survival and expansion in ER+ breast cancer. We conclude that SR co-activator complexes enhance CSC activity and therapy resistance by promoting metabolic plasticity. Inhibiting these complexes and/or associated binding partners in combination with endocrine therapies may be an effective strategy to block CSC survival and self-renewal, and breast cancer progression.

Our findings further implicate PELP1/SRC-3 complexes as mediators of CSC activity. We observed similarities in gene expression, cell metabolism, and sensitivity to inhibitors of PELP1

binding partners in endocrine and chemotherapy resistant ER+ cell lines. Although PELP1 expression contributes to cell survival in response to Taxol in TNBC (14), our studies are the first to demonstrate enhanced Taxol tolerance in the context of cyto PELP1 in ER+ breast cancer. Our results in TaxR models highlight the impact of targeting PELP1 binding partners involved in PELP1-mediated CSC self-renewal (**Figure 4**). Mesenchymal stem cells (27) and ovarian cancer cells (28) achieve Taxol resistance by shifting to G0 and entering quiescence. PELP1 is a substrate of CDKs and modulates G1/S cell cycle progression (29). PELP1 may confer Taxol resistance in part through cell cycle regulation, albeit further studies are needed to define cytoplasmic PELP1-specific contributions in this context.

Contributing factors to CSC survival include metabolic plasticity, which enables adaptation to diverse tumor environments. For example, inhibition of glycolysis reduces breast and lung CSCs (30). Glycolytic reprogramming has been documented in breast cancer cells during EMT, resulting in acquisition of CSC-like characteristics and tumorigenicity (31). In contrast, breast CSCs utilize oxidative phosphorylation (OXPHOS) as their primary metabolic program (32). Bulk tumor cells depend chiefly on glycolysis, whereas tumors enriched for breast CSCs rely mainly on OXPHOS (33). RNA-seq analysis indicated cytoplasmic PELP1 imparts increased HIF-activated pathways under normoxic 3D conditions to enrich for CSCs. ChIP assays demonstrated *EPAS1* (i.e. HIF-2α) recruitment to HRE regions of the PELP1 promoter in TNBC cells (34). Thus, PELP1-induced HIF pathways may serve as a feed-forward mechanism to drive metabolic genes programs. PFKFB3 and PFKFB4 are required for glycolytic response to hypoxia via HIF-1α activation (18). We demonstrated that cyto PELP1 expressing cells increased glycolysis and mitochondrial respiration. Additional studies are needed to define the bioenergetics driving this plasticity. PFKFB4-mediated SRC-3 Ser857 phosphorylation has essential functions in lung and breast cancer metastasis and metabolism (35). Phosphorylation of SRC-3 Ser857 promotes SRC-3 association with transcription factor *ATF4* to mediate non-oxidative pentose phosphate pathway and purine synthesis***.*** This study (35) did not evaluate SRC-3 in the context of CSCs, although SRC-3 has been linked to CSC activity (10,11). ATF4 pathway activation was identified by IPA in our studies (**Figure 1**) and could explain the correlation between PFKFB4 and PELP1/SRC-3-driven CSCs.

PFKFB inhibitors are emerging as promising treatments in endocrine and chemotherapy-resistant ER+ breast cancer (36). PFKFB3 inhibitor, PFK158, displays broad anti-tumor and immunomodulatory effects in human and preclinical mouse models (37) and was evaluated in a

Phase I clinical trial with no significant adverse effects (38). The prognostic value of PFKFB4 expression was evaluated in 200 tumor samples from stage I to III breast cancer patients. Similar to our METABRIC analysis (**Supplementary Figure 14**), elevated PFKFB4 expression was associated with poor disease-free survival and overall survival in ER+, HER2+, or TNBC patients (39). PFKFB4 inhibitors (e.g. 5MPN) have not yet moved to clinical trials. Studies have suggested correlative and mechanistic links between PFKFBs and CSCs. *PFKFB3* was upregulated in a $CD44^{hi}CD24^{lo}$ gene signature correlated to risk of distant metastasis and poor outcome in breast cancer patients (40). A cleaved product of CD44 (CD44ICD) promoted breast cancer stemness via PFKFB4-mediated glycolysis (41). Notably, 5MPN treatment suppressed CD44ICD-induced tumorigenesis. We have further implicated PFKFBs as drivers of CSC activity by demonstrating 5MPN reduces tumorspheres as a single agent or in combination treatments in multiple ER+ breast cancer models, including treatment resistant cells (TaxR, TamR), murine tumor cells, and pre-clinical PDxOs. Studies in breast cancer patients indicate that EMT and CSC markers are present in CTC populations, which have high metastatic potential. (42). Our MIND xenografts demonstrate PFKFB4 knockdown reduces CTC populations (**Figure 7**). These data suggest PFKFB4 inhibition is an effective strategy for targeting CSCs and CTCs in ER+ breast cancer. Future work should involve assessing overlap between PFKFB4-modulated CSC and CTC populations by evaluating the impact of 5MPN inhibitor combinations *in vivo*.

To evaluate the impact of SR co-activators on CSCs, it is important to consider ER-driven contributions. Breast CSCs are reported to be mostly ER negative (43), which may explain their poor response to anti-estrogens. However, SR+ cells contribute to CSC biology through SR-dependent (namely PR) paracrine factors (44)**.** For example, breast CSC self-renewal was stimulated after anti-estrogen treatment of breast cancer cells or PDX models (45,46). These studies suggest anti-estrogen therapies may initially slow tumor growth, but concurrently evoke plasticity and CSC activity in non-proliferative tumor cells. Notably, PELP1-containing complexes include ER and PR (47). PRs but not ER are potent drivers of stem and progenitor cell expansion in normal and neoplastic breast tissues (48). We have recently defined a requirement for phosphorylated and inducible PR in CSC biology (49,50), insulin hypersensitivity, and tam resistance in ER+ breast cancer (13). CSC outgrowth in therapy resistant ER+/PR-low breast cancer models is blocked by PR knockdown or antiprogestins (13). These findings suggest PELP1/SRC-3 complexes enable constitutive SR activity in sub-populations that easily bypass endocrine therapies. Antagonizing estrogen signaling may select for cells that display ligand-independent ER, resulting in increased proportions of breast CSCs, and subsequently promote

metastasis. Therefore, treatment should include endocrine therapy in combination with targeted therapies that block mediators of CSC survival and self-renewal as defined herein (i.e. PFKFBs).

CONCLUSION

Our work demonstrates that targeting SR co-activators and associated binding partners involved in driving CSC survival, self-renewal, and metabolic plasticity may impede breast cancer progression and has the potential to lead to improved outcomes. Identifying the mechanisms that mediate recurrent ER+ tumor cell populations (e.g. CSCs, CTCs) will enable specific targeting within heterogeneous breast tumors to overcome endocrine and chemotherapy resistance.

ACKNOWLEDGEMENTS

This work was supported by NIH grants R01 CA236948 (JHO, CAL), F32 CA210340 (THT), T32 HL007741 (THT), and U54 CA224076 (BWW), ACS Institutional Research Grant #124166-IRG-58-001-52-IRG5 (JHO), University of Minnesota Masonic Cancer Center (CAL, JHO), National Center for Advancing Translational Sciences of the NIH Award UL1TR000114 (JHO), and Department of Defense W81XWH-14-1-0417 (BWW). We thank Bruce Lindgren for biostatistics support, and the Masonic Cancer Center Biostatistics and Bioinformatics, Analytical Biochemistry, and Flow Cytometry shared resources. We also thank Zohar Sachs and Michael Franklin for critical reading of this manuscript.

FIGURE LEGENDS

Figure 1. PELP1-induced gene expression is altered in 3D conditions. (**A**) ALDH activity and (**B**) $CD44^{hi}/CD24^{lo}$ populations in MCF-7 PELP1 cells. (**C**) Venn diagrams showing unique genes up or downregulated >2-fold in MCF-7 PELP1 cells (3D vs. 2D). IPA analysis of (**D**) upstream regulators and (**E**) diseases or functions. (**F**) Representative heat-map showing log2(FPKM) values of cyto PELP1 gene signature. (**G**) Volcano plots of 3D vs. 2D comparison of MCF-7 PELP1 cells. X-axis is Log2(fold change) and Y-axis represent -Log 10 Benjamini-Hochberg corrected Q-values. Kaplan-Meier curves for upper and lower 50^{th} percentile of cyto PELP1 gene signature expression in the METABRIC (**H**) all subtypes and (**I**) ER+ only patient cohorts. Graphed data represent the mean ± SD (n = 3). * $p < 0.05$, ** $p < 0.01$, *** $p < 0.001$.

476 **Figure 2.** PELP1 cytoplasmic signaling upregulates HIF-activated metabolic pathways. (**A**) mRNA
477 levels of *EPAS1, PFKFB3, PFKFB4, NDRG1,* and *SOX9* in MCF-7 PELP1 cells. (**B**) OCR and
478 ECAR rates measured in MCF-7 PELP1 cells by Seahorse Cell Energy Phenotype test. (**C**) OCR
479 rates measured in MCF-7 PELP1 cells by Seahorse Mito Stress test. (**D**) Glucose uptake in cells
480 treated with 2-NBDG (10 μM). 2-NBDG uptake is represented as % cells relative to control.
481 Graphed data represent the mean ± SD (n = 3). * $p < 0.05$, ** $p < 0.01$, *** $p < 0.001$.
482
483 **Figure 3.** PFKFB inhibition blocks PELP1/SRC-3 signaling. Co-immunoprecipitation of (**A**) PELP1
484 and PFKFB3 or (**B**) PFKFB4 in MCF-7 PELP1 cells. Co-immunoprecipitation of PELP1 and SRC-
485 3 in MCF-7 PELP1 cells treated with vehicle (DMSO), (**C**) PFK158 (100 nM), or (**D**) 5MPN (5 μM).
486 Cell lysate controls (*right*). (**E**) Secondary tumorsphere assays in MCF-7 PELP1 shGFP control
487 or shPFKFB4 knockdown cells. Secondary tumorsphere assays in MCF-7 PELP1 cells treated
488 with vehicle, (**F**) PFK158 or (**G**) 5MPN. (**H**) Secondary tumorsphere assays in J110 cells treated
489 with vehicle, PFK158, or 5MPN. Western blot shows PFKFB3 and PFKFB4 protein in J110 cells.
490 Graphed data represent the mean ± SD (n = 3). * $p < 0.05$, ** $p < 0.01$, *** $p < 0.001$.
491
492 **Figure 4.** Therapy resistant models phenocopy cyto PELP1 cancer biology. (**A**) Taxol dose
493 response in MCF-7 PELP1 cells (0-125 nM Taxol). (**B**) mRNA levels of *EPAS1, PFKFB3*, and
494 *PFKFB4* in MCF-7 TaxR (*top*) or TamR (*bottom*) cells cultured in 2D or 3D conditions. (**C**) OCR
495 and ECAR rates measured in MCF-7 TaxR cells by Seahorse Cell Energy Phenotype test. (**D**)
496 OCR rates measured in MCF-7 TaxR cells by Seahorse Mito Stress test. (**E**) Glucose uptake in
497 cells treated with 2-NBDG (10 μM). (**F**) Co-immunoprecipitation of PELP1 and SRC-3 in MCF-7
498 TaxR (*top*) or TamR (*bottom*) cells. Secondary tumorsphere assays in (**G**) MCF-7 TaxR and (**H**)
499 MCF-7 TamR cells treated with vehicle (DMSO), PFK158 (100 nM), 5MPN (5 μM), or SI-2 (100
500 nM). Graphed data represent the mean ± SD (n = 3). * $p < 0.05$, ** $p < 0.01$, *** $p < 0.001$.
501
502 **Figure 5.** Endocrine therapies exhibit combinatorial effects with PELP1 complex inhibitors.
503 Tumorsphere assays in MCF-7 PELP1 cells treated with: (**A**) tam/SI-2, (**B**) tam/5MPN, or (**C**) SI-
504 2/5MPN. Tumorsphere assays in MCF-7 TaxR cells treated with: (**D**) tam/SI-2, (**E**) tam/5MPN, or
505 (**F**) SI-2/5MPN. Concentrations: tam (100 nM), 5MPN (5 μM), SI-2 (100 nM). Graphed data
506 represent the mean ± SD (n = 3). * $p < 0.05$, ** $p < 0.01$, *** $p < 0.001$.
507
508 **Figure 6.** Co-treatments in preclinical ER+ PDxO models target CSCs. (**A**) Western blot of
509 PELP1, SRC-3, PFKFB3, PFKFB4, and ER protein levels in HCI-003 and HCI-017. Tumorsphere

assays in HCI-003 and HCI-017 PDxOs co-treated with (**B**) tam/SI-2, (**C**) tam/5MPN, or (**D**) SI-2/5MPN. Prior to assay, PDxO models were pre-treated with the indicated compounds for 3 days and subjected to continued treatment during the assay. Concentrations: tam (100 nM), 5MPN (5 μM), SI-2 (100 nM). Graphed data represent the mean ± SD (n = 3). * $p < 0.05$, ** $p < 0.01$, *** $p < 0.001$.

Figure 7. PFKFB4 knockdown abrogates cyto PELP1 CTCs in MIND xenograft models. (**A**) Representative H&E stains from MIND glands (WT and cyto PELP1). (**B**) Tumor area (%) calculated from H&E sections from (**A**). (**C**) Tumor area (%) calculated from H&E sections from WT and cyto PELP1 (shGFP, shPFKFB4) MIND glands. (**D**) Representative images of CTCs from blood samples collected from mice injected with WT or cyto PELP1 (shGFP, shPFKFB4) cells. (**E**) Average size of soft agar colonies (CTCs) from (**D**). (**F**) Average number of colonies/well (CTCs). Graphed data represent the mean ± SD (n = 5). * $p < 0.05$, ** $p < 0.01$, *** $p < 0.001$

REFERENCES

1. Vadlamudi RK, Wang RA, Mazumdar A, Kim Y, Shin J, Sahin A, et al. Molecular cloning and characterization of PELP1, a novel human coregulator of estrogen receptor alpha. J Biol Chem 2001;276(41):38272-9.
2. Xu J, Liao L, Ning G, Yoshida-Komiya H, Deng C, O'Malley BW. The steroid receptor coactivator SRC-3 (p/CIP/RAC3/AIB1/ACTR/TRAM-1) is required for normal growth, puberty, female reproductive function, and mammary gland development. Proc Natl Acad Sci U S A 2000;97(12):6379-84.
3. Habashy HO, Powe DG, Rakha EA, Ball G, Macmillan RD, Green AR, et al. The prognostic significance of PELP1 expression in invasive breast cancer with emphasis on the ER-positive luminal-like subtype. Breast Cancer Res Treat 2010;120(3):603-12.
4. Kumar R, Zhang H, Holm C, Vadlamudi RK, Landberg G, Rayala SK. Extranuclear coactivator signaling confers insensitivity to tamoxifen. Clin Cancer Res 2009;15(12):4123-30.
5. Vadlamudi RK, Manavathi B, Balasenthil S, Nair SS, Yang Z, Sahin AA, et al. Functional implications of altered subcellular localization of PELP1 in breast cancer cells. Cancer Res 2005;65(17):7724-32.
6. Burandt E, Jens G, Holst F, Janicke F, Muller V, Quaas A, et al. Prognostic relevance of AIB1 (NCoA3) amplification and overexpression in breast cancer. Breast Cancer Res Treat 2013;137(3):745-53.
7. Louie MC, Zou JX, Rabinovich A, Chen HW. ACTR/AIB1 functions as an E2F1 coactivator to promote breast cancer cell proliferation and antiestrogen resistance. Mol Cell Biol 2004;24(12):5157-71.

8. Osborne CK, Bardou V, Hopp TA, Chamness GC, Hilsenbeck SG, Fuqua SA, et al. Role of the estrogen receptor coactivator AIB1 (SRC-3) and HER-2/neu in tamoxifen resistance in breast cancer. J Natl Cancer Inst 2003;95(5):353-61.
9. Visvader JE, Lindeman GJ. Cancer stem cells: current status and evolving complexities. Cell Stem Cell 2012;10(6):717-28.
10. Rohira AD, Yan F, Wang L, Wang J, Zhou S, Lu A, et al. Targeting SRC Coactivators Blocks the Tumor-Initiating Capacity of Cancer Stem-like Cells. Cancer Res 2017;77(16):4293-304.
11. Truong TH, Hu H, Temiz NA, Hagen KM, Girard BJ, Brady NJ, et al. Cancer Stem Cell Phenotypes in ER(+) Breast Cancer Models Are Promoted by PELP1/AIB1 Complexes. Mol Cancer Res 2018;16(4):707-19.
12. Yang Y, Chan JY, Temiz NA, Yee D. Insulin Receptor Substrate Suppression by the Tyrphostin NT157 Inhibits Responses to Insulin-Like Growth Factor-I and Insulin in Breast Cancer Cells. Horm Cancer 2018;9(6):371-82.
13. Dwyer AR, Truong TH, Perez Kerkvliet C, Paul KV, Kabos P, Sartorius CA, et al. Insulin Receptor Substrate-1 (IRS-1) Mediates Progesterone Receptor-Driven Stemness and Endocrine Resistance in Estrogen Receptor+ Breast Cancer Br J Cancer 2020;Manuscript Accepted.
14. Regan Anderson TM, Ma S, Perez Kerkvliet C, Peng Y, Helle TM, Krutilina RI, et al. Taxol Induces Brk-dependent Prosurvival Phenotypes in TNBC Cells through an AhR/GR/HIF-driven Signaling Axis. Mol Cancer Res 2018;16(11):1761-72.
15. Behbod F, Kittrell FS, LaMarca H, Edwards D, Kerbawy S, Heestand JC, et al. An intraductal human-in-mouse transplantation model mimics the subtypes of ductal carcinoma in situ. Breast Cancer Res 2009;11(5):R66.
16. Sflomos G, Dormoy V, Metsalu T, Jeitziner R, Battista L, Scabia V, et al. A Preclinical Model for ERalpha-Positive Breast Cancer Points to the Epithelial Microenvironment as Determinant of Luminal Phenotype and Hormone Response. Cancer Cell 2016;29(3):407-22.
17. Liu Y, Nenutil R, Appleyard MV, Murray K, Boylan M, Thompson AM, et al. Lack of correlation of stem cell markers in breast cancer stem cells. Br J Cancer 2014;110(8):2063-71.
18. Chesney J, Clark J, Klarer AC, Imbert-Fernandez Y, Lane AN, Telang S. Fructose-2,6-bisphosphate synthesis by 6-phosphofructo-2-kinase/fructose-2,6-bisphosphatase 4 (PFKFB4) is required for the glycolytic response to hypoxia and tumor growth. Oncotarget 2014;5(16):6670-86.
19. Kim JW, Dang CV. Cancer's molecular sweet tooth and the Warburg effect. Cancer Res 2006;66(18):8927-30.
20. Shi L, Pan H, Liu Z, Xie J, Han W. Roles of PFKFB3 in cancer. Signal Transduct Target Ther 2017;2:17044.
21. Torres-Arzayus MI, Font de Mora J, Yuan J, Vazquez F, Bronson R, Rue M, et al. High tumor incidence and activation of the PI3K/AKT pathway in transgenic mice define AIB1 as an oncogene. Cancer Cell 2004;6(3):263-74.

22. Torres-Arzayus MI, Yuan J, DellaGatta JL, Lane H, Kung AL, Brown M. Targeting the AIB1 oncogene through mammalian target of rapamycin inhibition in the mammary gland. Cancer Res 2006;66(23):11381-8.
23. Guillen KP, Fujita M, Butterfield AJ, Welm BW. Manuscript in Preparation. 2020.
24. Kilgour E, Rothwell DG, Brady G, Dive C. Liquid Biopsy-Based Biomarkers of Treatment Response and Resistance. Cancer Cell 2020;37(4):485-95.
25. Budd GT, Cristofanilli M, Ellis MJ, Stopeck A, Borden E, Miller MC, et al. Circulating tumor cells versus imaging--predicting overall survival in metastatic breast cancer. Clin Cancer Res 2006;12(21):6403-9.
26. Moore N, Lyle S. Quiescent, slow-cycling stem cell populations in cancer: a review of the evidence and discussion of significance. J Oncol 2011;2011.
27. Bosco DB, Kenworthy R, Zorio DA, Sang QX. Human mesenchymal stem cells are resistant to Paclitaxel by adopting a non-proliferative fibroblastic state. PLoS One 2015;10(6):e0128511.
28. Wang X, Pan L, Mao N, Sun L, Qin X, Yin J. Cell-cycle synchronization reverses Taxol resistance of human ovarian cancer cell lines. Cancer Cell Int 2013;13(1):77.
29. Nair BC, Nair SS, Chakravarty D, Challa R, Manavathi B, Yew PR, et al. Cyclin-dependent kinase-mediated phosphorylation plays a critical role in the oncogenic functions of PELP1. Cancer Res 2010;70(18):7166-75.
30. O'Neill S, Porter RK, McNamee N, Martinez VG, O'Driscoll L. 2-Deoxy-D-Glucose inhibits aggressive triple-negative breast cancer cells by targeting glycolysis and the cancer stem cell phenotype. Sci Rep 2019;9(1):3788.
31. Dong C, Yuan T, Wu Y, Wang Y, Fan TW, Miriyala S, et al. Loss of FBP1 by Snail-mediated repression provides metabolic advantages in basal-like breast cancer. Cancer Cell 2013;23(3):316-31.
32. Vlashi E, Lagadec C, Vergnes L, Reue K, Frohnen P, Chan M, et al. Metabolic differences in breast cancer stem cells and differentiated progeny. Breast Cancer Res Treat 2014;146(3):525-34.
33. Banerjee A, Arvinrad P, Darley M, Laversin SA, Parker R, Rose-Zerilli MJJ, et al. The effects of restricted glycolysis on stem-cell like characteristics of breast cancer cells. Oncotarget 2018;9(33):23274-88.
34. Regan Anderson TM, Ma SH, Raj GV, Cidlowski JA, Helle TM, Knutson TP, et al. Breast Tumor Kinase (Brk/PTK6) Is Induced by HIF, Glucocorticoid Receptor, and PELP1-Mediated Stress Signaling in Triple-Negative Breast Cancer. Cancer Res 2016;76(6):1653-63.
35. Dasgupta S, Rajapakshe K, Zhu B, Nikolai BC, Yi P, Putluri N, et al. Metabolic enzyme PFKFB4 activates transcriptional coactivator SRC-3 to drive breast cancer. Nature 2018;556(7700):249-54.
36. Mondal S, Roy D, Sarkar Bhattacharya S, Jin L, Jung D, Zhang S, et al. Therapeutic targeting of PFKFB3 with a novel glycolytic inhibitor PFK158 promotes lipophagy and chemosensitivity in gynecologic cancers. Int J Cancer 2019;144(1):178-89.
37. Telang S, Yaddanapudi K, Grewal J, Redman R, Fu S, Pohlmann P, et al. Abstract B90: PFK-158 is a first-in-human inhibitor of PFKFB3 that selectively suppresses glucose

metabolism of cancer cells and inhibits the immunosuppressive Th17 cells and MDSCs in advanced cancer patients. Cancer Res 2016;76(24 Supplement):B90.

38. Redman R, Pohlmann P, Kurman M, Tapolsky GH, Chesney J. Abstract CT206: PFK-158, first-in-man and first-in-class inhibitor of PFKFB3/ glycolysis: A phase I, dose escalation, multi-center study in patients with advanced solid malignancies. Cancer Res 2015;75(15 Supplement):CT206.

39. Yao L, Wang L, Cao ZG, Hu X, Shao ZM. High expression of metabolic enzyme PFKFB4 is associated with poor prognosis of operable breast cancer. Cancer Cell Int 2019;19:165.

40. Marotta LL, Almendro V, Marusyk A, Shipitsin M, Schemme J, Walker SR, et al. The JAK2/STAT3 signaling pathway is required for growth of CD44(+)CD24(-) stem cell-like breast cancer cells in human tumors. J Clin Invest 2011;121(7):2723-35.

41. Gao R, Li D, Xun J, Zhou W, Li J, Wang J, et al. CD44ICD promotes breast cancer stemness via PFKFB4-mediated glucose metabolism. Theranostics 2018;8(22):6248-62.

42. Giordano A, Gao H, Anfossi S, Cohen E, Mego M, Lee BN, et al. Epithelial-mesenchymal transition and stem cell markers in patients with HER2-positive metastatic breast cancer. Mol Cancer Ther 2012;11(11):2526-34.

43. Harrison H, Simoes BM, Rogerson L, Howell SJ, Landberg G, Clarke RB. Oestrogen increases the activity of oestrogen receptor negative breast cancer stem cells through paracrine EGFR and Notch signalling. Breast Cancer Res 2013;15(2):R21.

44. Joshi PA, Jackson HW, Beristain AG, Di Grappa MA, Mote PA, Clarke CL, et al. Progesterone induces adult mammary stem cell expansion. Nature 2010;465(7299):803-7.

45. Simoes BM, O'Brien CS, Eyre R, Silva A, Yu L, Sarmiento-Castro A, et al. Anti-estrogen Resistance in Human Breast Tumors Is Driven by JAG1-NOTCH4-Dependent Cancer Stem Cell Activity. Cell Rep 2015;12(12):1968-77.

46. Shea MP, O'Leary KA, Fakhraldeen SA, Goffin V, Friedl A, Wisinski KB, et al. Antiestrogen Therapy Increases Plasticity and Cancer Stemness of Prolactin-Induced ERalpha(+) Mammary Carcinomas. Cancer Res 2018;78(7):1672-84.

47. Daniel AR, Gaviglio AL, Knutson TP, Ostrander JH, D'Assoro AB, Ravindranathan P, et al. Progesterone receptor-B enhances estrogen responsiveness of breast cancer cells via scaffolding PELP1- and estrogen receptor-containing transcription complexes. Oncogene 2015;34(4):506-15.

48. Rajaram RD, Buric D, Caikovski M, Ayyanan A, Rougemont J, Shan J, et al. Progesterone and Wnt4 control mammary stem cells via myoepithelial crosstalk. EMBO J 2015;34(5):641-52.

49. Knutson TP, Truong TH, Ma S, Brady NJ, Sullivan ME, Raj G, et al. Posttranslationally modified progesterone receptors direct ligand-specific expression of breast cancer stem cell-associated gene programs. J Hematol Oncol 2017;10(1):89.

50. Truong TH, Dwyer AR, Diep CH, Hu H, Hagen KM, Lange CA. Phosphorylated Progesterone Receptor Isoforms Mediate Opposing Stem Cell and Proliferative Breast Cancer Cell Fates. Endocrinology 2019;160(2):430-46.

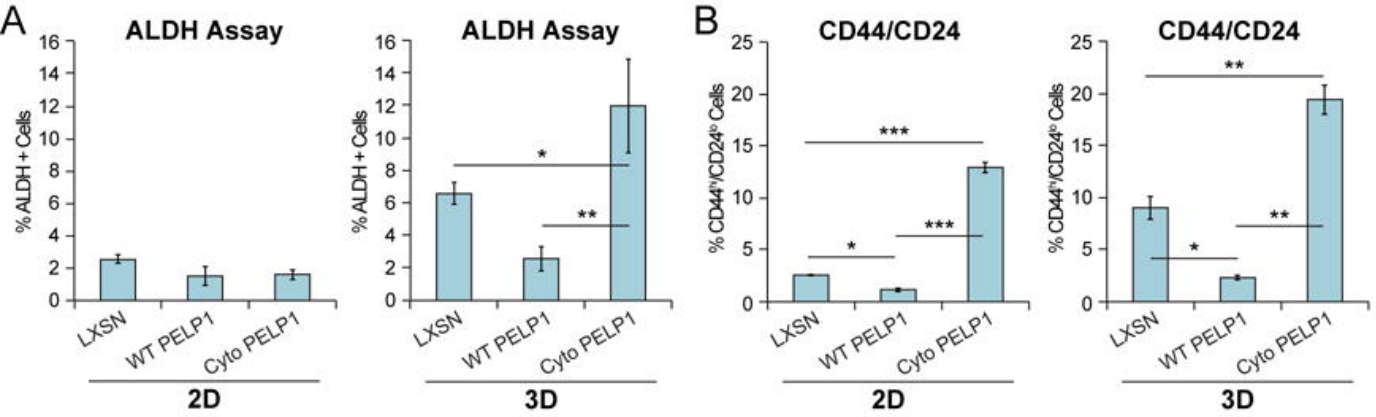

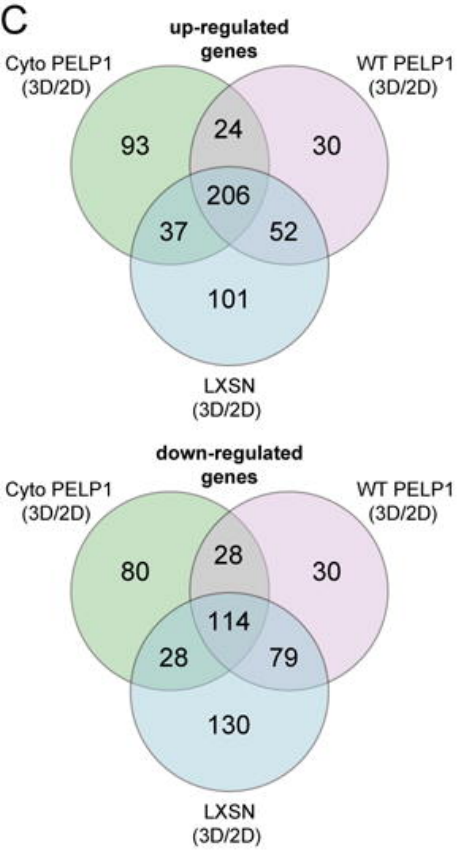

D

Upstream Regulator	Predicted Activation State	Activation z-score	p-value of overlap
HIF1A	Activated	2.787	6.05E-11
beta-estradiol	Activated	2.923	7.61E-11
EPAS1	Activated	2.373	9.12E-07
ATF4	Activated	2.558	3.32E-06
ARNT	Activated	2.407	3.63E-06
Hif1	Activated	2.200	7.28E-06
CD38	Activated	2.789	2.77E-05
cobalt chloride	Activated	2.403	3.34E-05
IL5	Activated	2.53	6.05E-05
Gsk3	Activated	2.167	3.24E-04
salirasib	Inhibited	-2.138	5.15E-09
VHL	Inhibited	-2.153	7.67E-07
EGLN	Inhibited	-2.909	3.49E-06
fulvestrant	Inhibited	-2.123	1.82E-04
SAHM1	Inhibited	-2.000	2.62E-04

E

Diseases or Functions Annotation	Predicted Activation State	Activation z-score	p-value
Metastatic solid tumor	Increased	2.404	2.50E-05
Visceral metastasis	Increased	2.200	2.52E-05
Quantity of amino acids	Increased	2.082	2.30E-04
Glycolysis of cells	Increased	2.183	5.90E-04
Glucose metabolism disorder	Decreased	-2.285	7.16E-07
Release of vesicles	Decreased	-2.000	2.51E-04
Apoptosis of neuroblastoma cell lines	Decreased	-2.175	5.02E-04

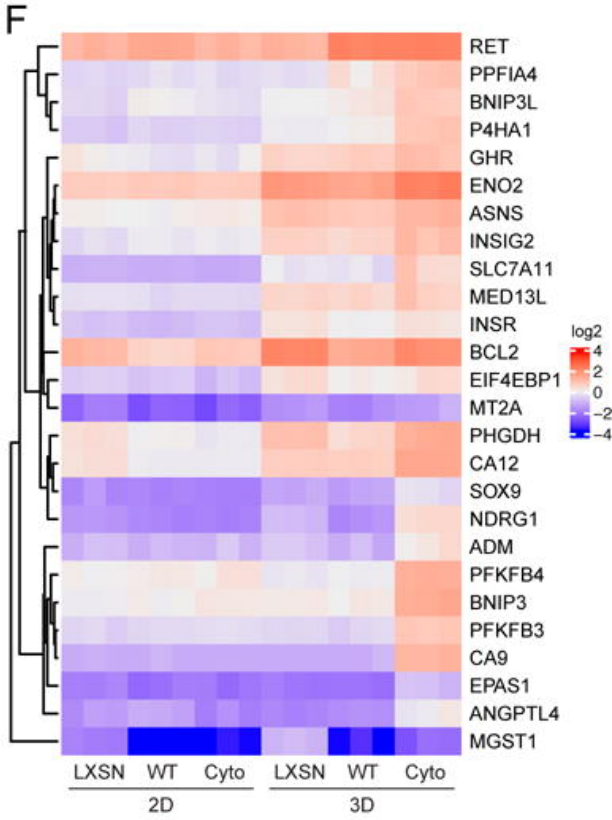

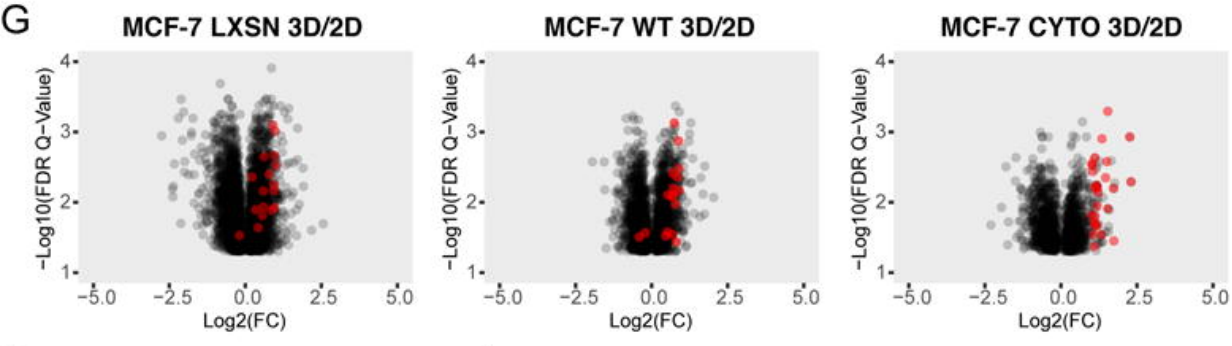

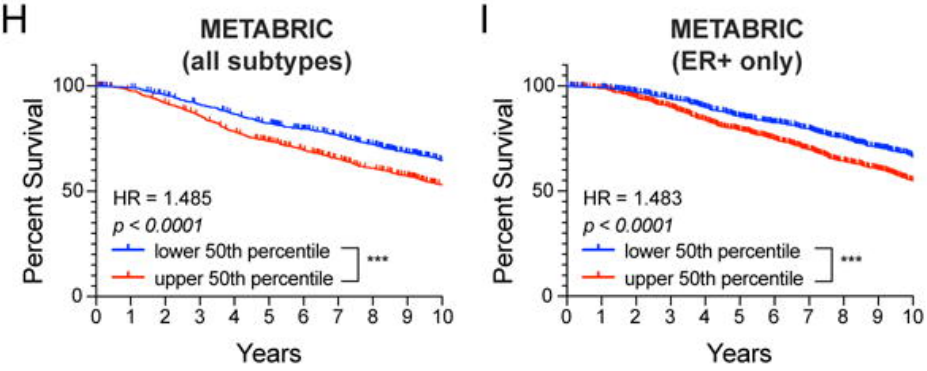

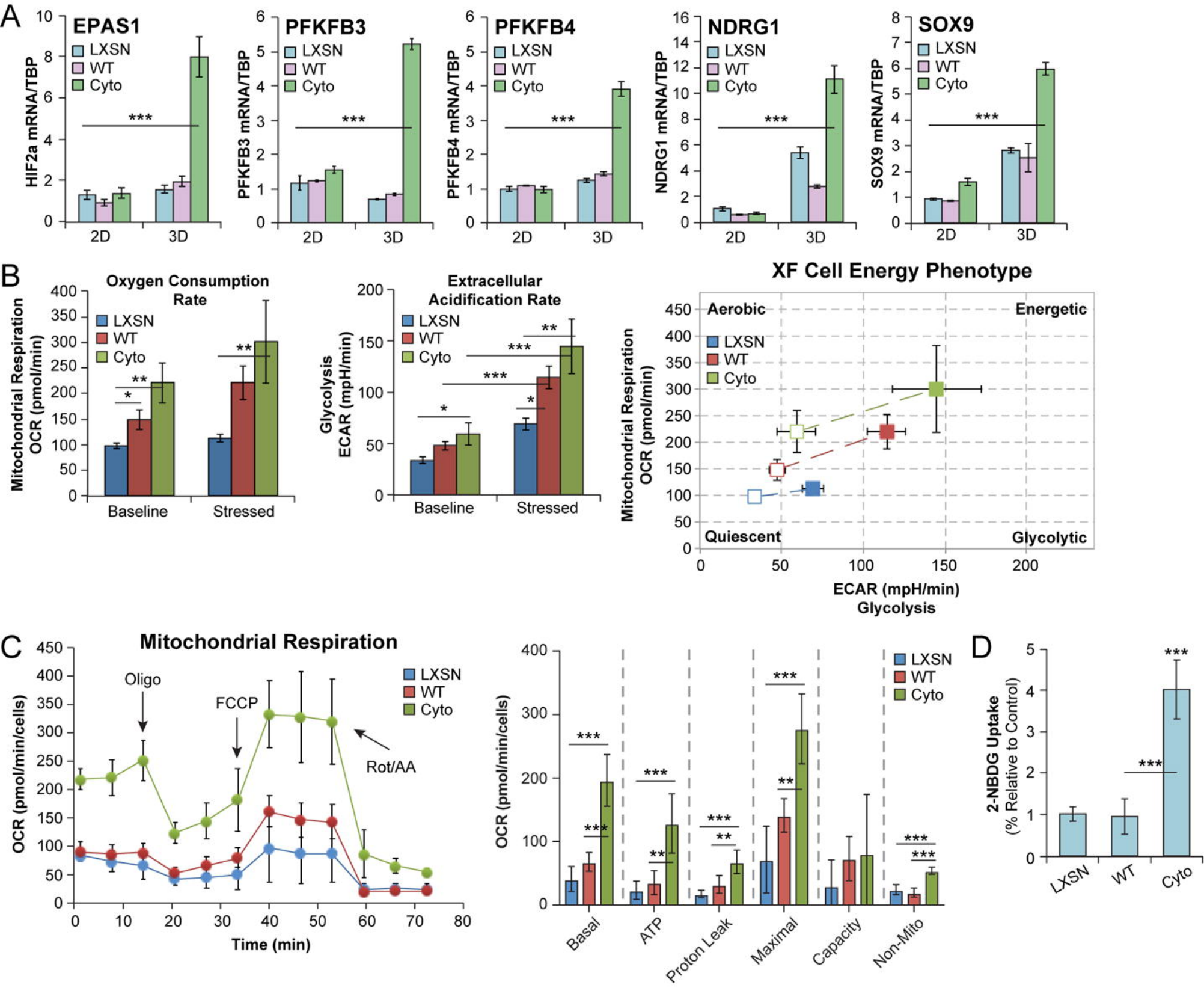
A
EPAS1
PFKFB3
PFKFB4
NDRG1
SOX9
LXSN
WT
Cyto
HIF2a mRNA/TBP
PFKFB3 mRNA/TBP
PFKFB4 mRNA/TBP
NDRG1 mRNA/TBP
SOX9 mRNA/TBP
***
2D
3D
B
Oxygen Consumption Rate
Mitochondrial Respiration OCR (pmol/min)
Extracellular Acidification Rate
Glycolysis ECAR (mpH/min)
Baseline
Stressed
XF Cell Energy Phenotype
Aerobic
Energetic
Quiescent
Glycolytic
ECAR (mpH/min) Glycolysis
C
Mitochondrial Respiration
Oligo
FCCP
Rot/AA
OCR (pmol/min/cells)
Time (min)
Basal
ATP
Proton Leak
Maximal
Capacity
Non-Mito
D
2-NBDG Uptake
(% Relative to Control)

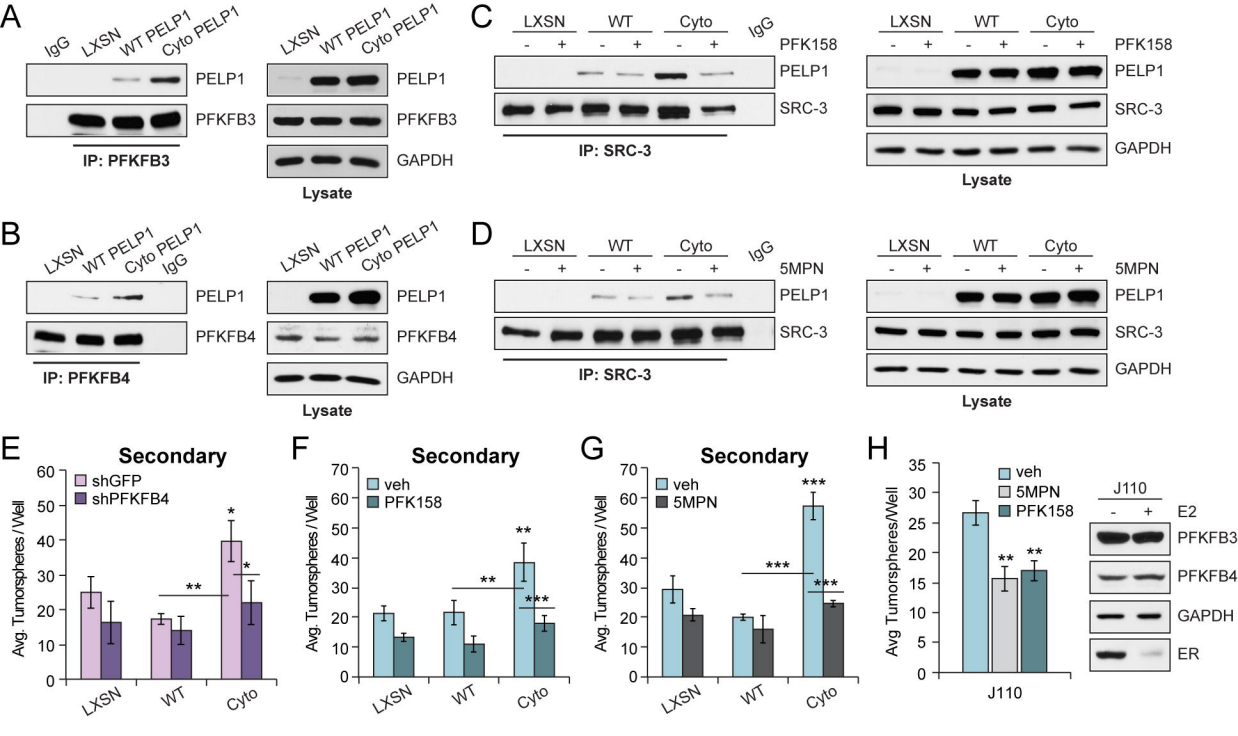
A
IgG
LXSN
WT PELP1
Cyto PELP1
PELP1
PFKFB3
IP: PFKFB3
GAPDH
Lysate
B
PFKFB4
IP: PFKFB4
C
LXSN
WT
Cyto
IgG
PFK158
SRC-3
IP: SRC-3
D
5MPN
E
Secondary
shGFP
shPFKFB4
Avg. Tumorspheres / Well
F
veh
PFK158
G
5MPN
H
J110
E2
ER

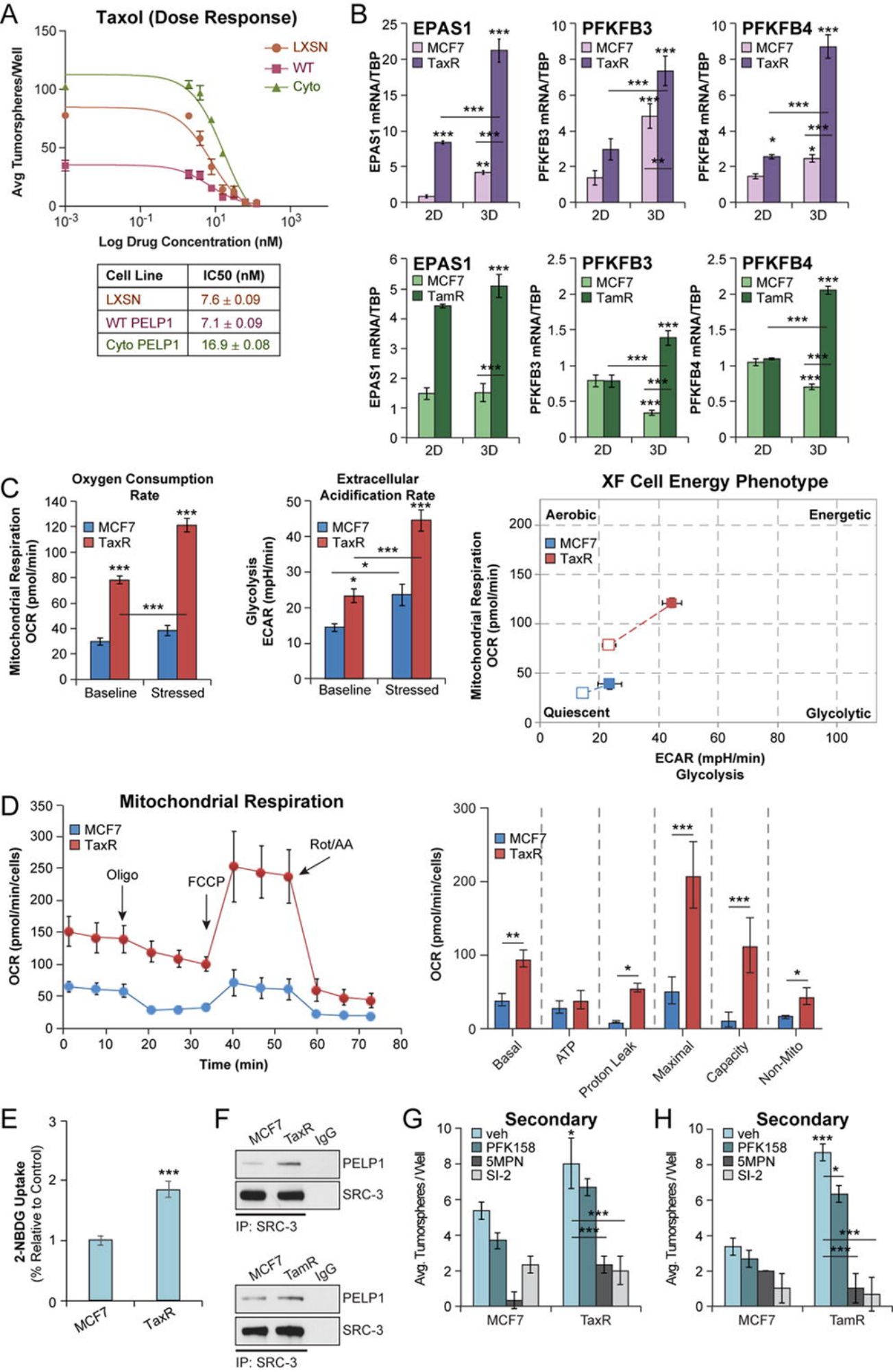
A
Taxol (Dose Response)
LXSN
WT
Cyto
Avg Tumorspheres/Well
Log Drug Concentration (nM)
Cell Line | IC50 (nM)
LXSN | 7.6 ± 0.09
WT PELP1 | 7.1 ± 0.09
Cyto PELP1 | 16.9 ± 0.08
B
EPAS1
PFKFB3
PFKFB4
MCF7
TaxR
TamR
EPAS1 mRNA/TBP
PFKFB3 mRNA/TBP
PFKFB4 mRNA/TBP
2D
3D
C
Oxygen Consumption Rate
Mitochondrial Respiration OCR (pmol/min)
Extracellular Acidification Rate
Glycolysis ECAR (mpH/min)
Baseline
Stressed
XF Cell Energy Phenotype
Aerobic
Energetic
Quiescent
Glycolytic
ECAR (mpH/min) Glycolysis
D
Mitochondrial Respiration
OCR (pmol/min/cells)
Oligo
FCCP
Rot/AA
Time (min)
Basal
ATP
Proton Leak
Maximal
Capacity
Non-Mito
E
2-NBDG Uptake (% Relative to Control)
F
IgG
PELP1
SRC-3
IP: SRC-3
G
Secondary
veh
PFK158
5MPN
SI-2
Avg. Tumorspheres/Well
H

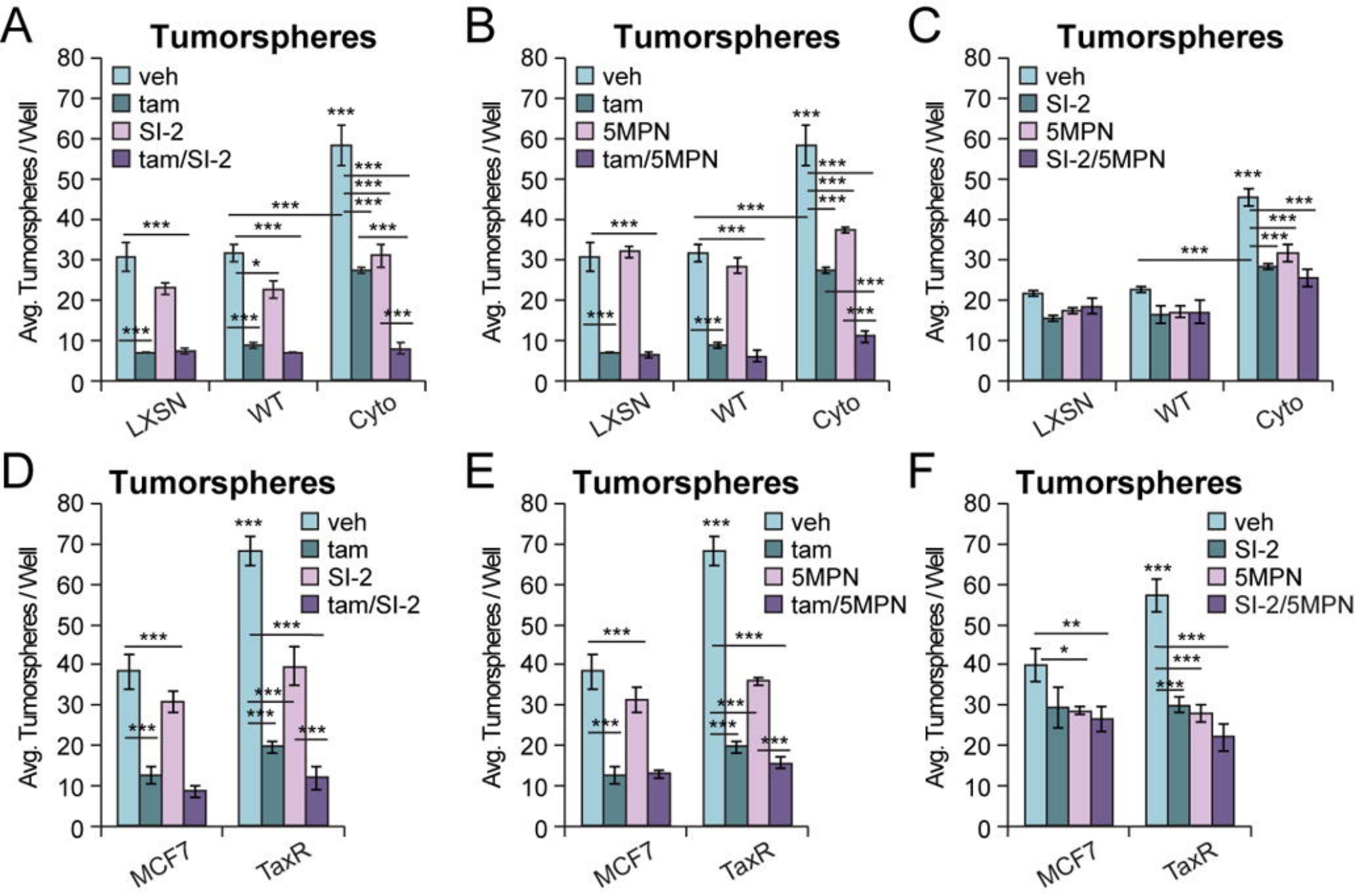
A
Tumorspheres
Avg. Tumorspheres / Well
veh
tam
SI-2
tam/SI-2
LXSN
WT
Cyto
B
Tumorspheres
Avg. Tumorspheres / Well
veh
tam
5MPN
tam/5MPN
LXSN
WT
Cyto
C
Tumorspheres
Avg. Tumorspheres / Well
veh
SI-2
5MPN
SI-2/5MPN
LXSN
WT
Cyto
D
Tumorspheres
Avg. Tumorspheres / Well
veh
tam
SI-2
tam/SI-2
MCF7
TaxR
E
Tumorspheres
Avg. Tumorspheres / Well
veh
tam
5MPN
tam/5MPN
MCF7
TaxR
F
Tumorspheres
Avg. Tumorspheres / Well
veh
SI-2
5MPN
SI-2/5MPN
MCF7
TaxR

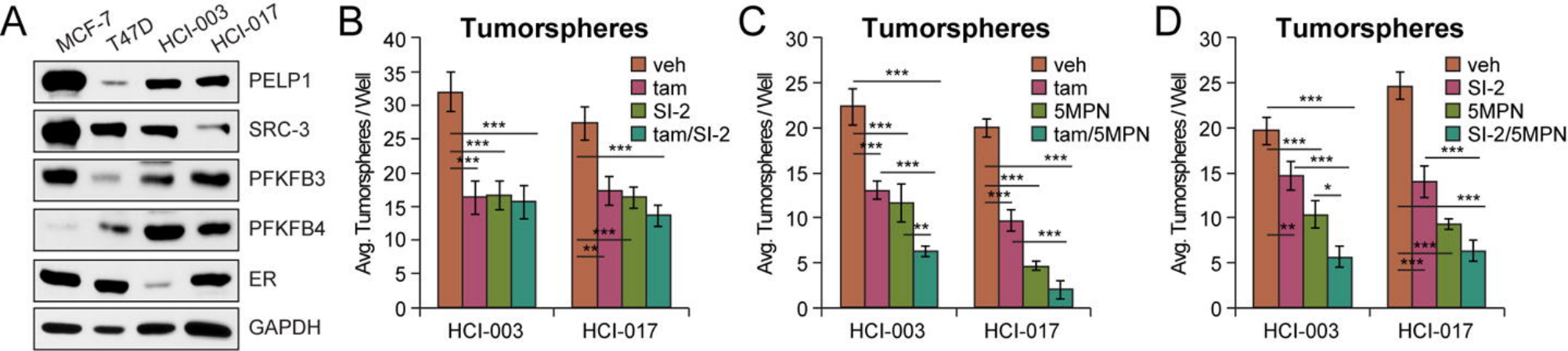
A
MCF-7
T47D
HCI-003
HCI-017
PELP1
SRC-3
PFKFB3
PFKFB4
ER
GAPDH
B
Tumorspheres
Avg. Tumorspheres / Well
veh
tam
SI-2
tam/SI-2
HCI-003
HCI-017
C
Tumorspheres
Avg. Tumorspheres / Well
veh
tam
5MPN
tam/5MPN
HCI-003
HCI-017
D
Tumorspheres
Avg. Tumorspheres / Well
veh
SI-2
5MPN
SI-2/5MPN
HCI-003
HCI-017

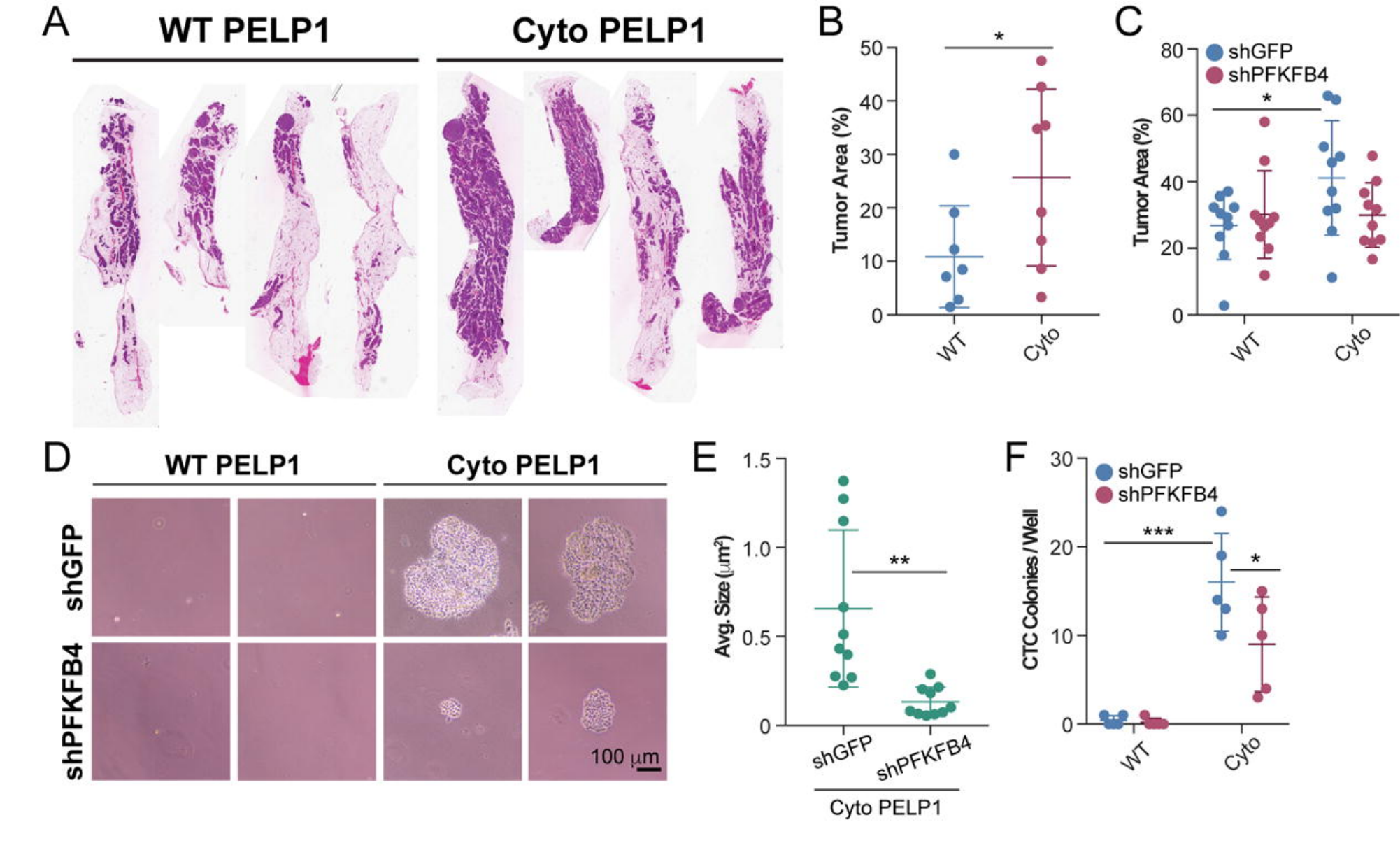
A
WT PELP1
Cyto PELP1
B
Tumor Area (%)
50
40
30
20
10
0
*
WT
Cyto
C
shGFP
shPFKFB4
Tumor Area (%)
80
60
40
20
0
*
WT
Cyto
D
WT PELP1
Cyto PELP1
shGFP
shPFKFB4
100 μm
E
Avg. Size (μm²)
1.5
1.0
0.5
0
**
shGFP
shPFKFB4
Cyto PELP1
F
shGFP
shPFKFB4
CTC Colonies / Well
30
20
10
0
***
*
WT
Cyto